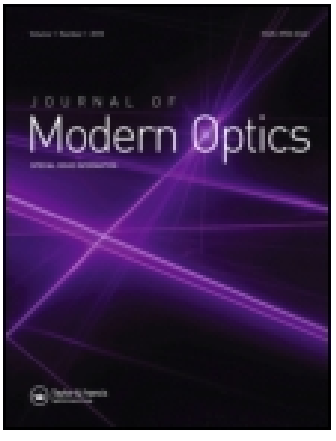

Journal of Modern Optics
Publication details, including instructions for authors and subscription information:
http://www.tandfonline.com/loi/tmop20

All fiber on-axis coupling scheme between single mode fiber and GRIN fiber

Waleed S. Mohammed [a], Xija Gu [b], Joachim Meier [a] & Peter W.E. Smith [a]

[a] Electronic and Computer Engineering Department, University of Toronto, Toronto, Canada

[b] Electronic and Computer Engineering Department, Ryerson University, Toronto, Canada

Published online: 12 May 2008.

To cite this article: Waleed S. Mohammed, Xija Gu, Joachim Meier & Peter W.E. Smith (2008) All fiber on-axis coupling scheme between single mode fiber and GRIN fiber, Journal of Modern Optics, 55:7, 1033-1049, DOI: 10.1080/09500340701558542

To link to this article: http://dx.doi.org/10.1080/09500340701558542

Journal of Modern Optics
Vol. 55, No. 7, 10 April 2008, 1033–1049

Taylor & Francis
Taylor & Francis Group

All fiber on-axis coupling scheme between single mode fiber and GRIN fiber

Waleed S. Mohammed[a]*, Xija Gu[b], Joachim Meier[a] and Peter W.E. Smith[a]

[a]*Electronic and Computer Engineering Department, University of Toronto, Toronto, Canada;* [b]*Electronic and Computer Engineering Department, Ryerson University, Toronto, Canada*

(*Received 12 February 2007; revised 4 July 2007*)

In this paper we present a simple and novel method to maximize on-axis coupling efficiency to radially symmetric fibers without the need for extra free space optical elements. The method is based on inserting a segment of step-index multimode fiber (MMF), cleaved to a particular length, between the input fiber and the output fiber (OF). The MMF segment modifies the input field to match the guided modes in the OF. Using this technique we show that, by inserting an appropriate length MMF segment, it is theoretically possible to obtain a coupling coefficient as high as −0.8 dB between a single mode fiber and a graded index ring-shaped fiber and −0.32 dB for a multi-shell fiber. Our experimental measurements showed good agreement with theoretical predictions for the ring fiber.

Keywords: optical fiber; fiber coupling; multimode interference; specialty fiber

1. Introduction

Cylindrical symmetric fibers with different index profiles are widely used for a variety of applications such as light delivery, sensing and biomedical applications [1–4]. Efficient coupling to these fibers is an important issue. In previous work this was achieved using an external diffractive optical element, such as a vortex lens, to selectively excite higher order azimuthal modes in graded index (GRIN) fibers [5]. We presented in previous work the use of a subwavelength grating structure to selectively excite the TE01 mode in a hollow glass fiber [6]. These previous methods introduced free space optical elements and, in some cases extra coupling lenses, to couple light out of the source fiber into the output fiber (OF). Alignment is a critical issue in these methods. One way to avoid the need for external elements is a direct off-axis butt coupling with the source fiber. This off-axis coupling will excite higher order azimuthal modes in GRIN fibers and maximize the power coupled to fibers with ring-shaped guiding regions. However, for reasons of simplicity and reliability, it is always desirable to have an on-axis all-fiber coupling scheme.

ISSN 0950–0340 print/ISSN 1362–3044 online

DOI: 10.1080/09500340701558542
http://www.informaworld.com

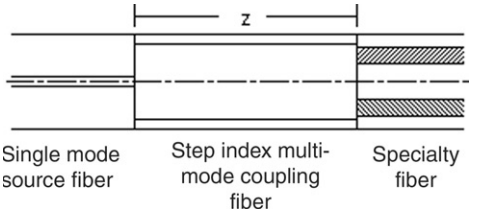

Figure 1. The general coupling scheme.

In this paper, we present a novel technique to maximize the on-axis coupling between a single mode fiber (SMF) and a general cylindrical symmetric output fiber by inserting a segment of a step-index multimode fiber (MMF) between the two fibers as depicted in Figure 1. This segment works as a beam shaping element. The light from the source fiber excites several modes inside the MMF, which interfere during propagation. This well-known effect is referred to as multi-mode interference (MMI) [7]. MMI causes the transverse complex field profile to vary along the fiber axis. This effect can be used for several applications by properly selecting the MMF parameters. In [4] we used a MMF spliced to a SMF as a displacement sensor. The same device was used as a wavelength tunable fiber lens [8]. In another application, this effect was used by Selvas et al. to fabricate a cheap and compact wavelength tunable fiber laser [9]. In other applications, the MMI in the fiber was used to enhance the tuning mechanism in fiber lasers [10] and as a temperature sensor [11].

We focus on using the MMI effect to maximize the power coupling between a single mode fiber and an arbitrary index profile cylindrically-symmetric OF. The basic concept of the proposed scheme is to properly select the MMF parameters such that the transverse field profile at the end of it is highly correlated to the guided modes inside the output fiber. This correlation is calculated through the well-known overlap coupling relation. Although the MMI effect inside the fiber and the coupling calculations were thoroughly studied, in Section 2 we present some detailed theoretical derivation of the total power coupling efficiency to a general OF when using a MMF segment. The theoretical derivations are carried out to stress essential design key elements and to guarantee understanding of the proposed scheme. Section 3 illustrates the use of this scheme to maximize the coupling efficiency to two different fiber systems; ring-shaped GRIN fiber and multi-shell fiber.

2. Theory

At a certain wavelength, the field of the source fiber excites several guided modes inside the MMF. The source transverse field distribution E_s at the input facet of the MMF can be written as an infinite summation of the transverse fields of the guided, cladding and radiation modes inside the MMF. For a large core radius and long enough MMF segment the problem can be simplified to a finite summation over the guided modes only, as increasing the MMF core size increases the number of guided modes and hence, increases

the confinement and minimizes the power in the cladding modes [12]. Under these circumstances we can write:

$$\boldsymbol{E}_{\mathrm{s}}(r,\theta) = \sum_{j=0}^{M-1} a_j \cdot E_j^{\mathrm{t}}(r,\theta), \tag{1}$$

where E_j^{t} and a_j are the jth mode transverse electric field vector and field expansion coefficient, respectively. r and θ are the radial and athimuthal coordinates. The constant M is the total number of guided modes inside the MMF. The field expansion coefficient in Equation (1) is calculated from the orthogonality condition between the guided modes of the fiber (see Appendix A for detailed derivation):

$$a_j = \frac{\int_{r=0}^{\infty}\int_{\theta=0}^{2\pi} \boldsymbol{E}_{\mathrm{s}}(r,\theta) \times H_j^{\mathrm{t}^*}(r,\theta) r \,\mathrm{d}r \,\mathrm{d}\theta}{P_j}, \tag{2}$$

where H_j^{t} is the jth mode transverse magnetic field and P_j is the jth mode power defined by Equation (A7). We define a modified expansion coefficient $\tilde{a}_j$,

$$\tilde{a}_j = \frac{\int_{r=0}^{\infty}\int_{\theta=0}^{2\pi} \boldsymbol{E}_{\mathrm{s}}(r,\theta) \times H_j^{\mathrm{t}^*}(r,\theta) r \,\mathrm{d}r \,\mathrm{d}\theta}{(P_j P_s)^{1/2}} = a_j \left(\frac{P_j}{P_s}\right)^{1/2}, \tag{3}$$

where P_s is the source power defined by Equation (A9). This modified expansion coefficient is selected as it is directly related to the mode power coupling coefficient, η_j (Equation (A10)), through the following relation

$$\eta_j = |\tilde{a}_j|^2. \tag{4}$$

Using the field representation in Equation (1), the electric field distribution at any location z along the fiber, $\boldsymbol{E}_{\mathrm{MMF}}(r, \theta, z)$, can be written as a superposition of the guided mode fields scaled by the expansion coefficient $\tilde{\mathrm{a}}_j$ and a linear phase term, $\exp(\mathrm{i}\beta_j z)$, where β_j is the jth mode longitudinal propagation constant, i.e.

$$\boldsymbol{E}_{\mathrm{MMF}}(r,\theta,z) = \sum_{j=0}^{M-1} \tilde{a}_j \left(\frac{P_s}{P_j}\right)^{1/2} E_j^{\mathrm{t}}(r,\theta) \exp(\mathrm{i}\beta_j z). \tag{5}$$

Similarly, the magnetic field distribution, $\boldsymbol{H}_{\mathrm{MMF}}(r, \theta, z)$, gives:

$$\boldsymbol{H}_{\mathrm{MMF}}(r,\theta,z) = \sum_{j=0}^{M-1} \tilde{a}_j \left(\frac{P_s}{P_j}\right)^{1/2} H_j^{\mathrm{t}}(r,\theta) \exp(\mathrm{i}\beta_j z). \tag{6}$$

Equations (5) and (6) show that the transverse complex field distribution at any distance z within the fiber can be calculated directly through the superposition of the MMF modes weighted by the expansion coefficients, a_j, and phase modulated by the propagation constant of each mode, β_j multiplied by z. At the end facet of the MMF segment, the output fields (Equations (5) and (6)) depend on the source excitation condition, the length and the modal properties of the MMF. The modal properties depend on the excitation

wavelength, fiber core size and core and cladding materials. Fixing the fiber materials, the transverse field distribution then becomes only a function of three parameters: source excitation condition, core radius and segment length. Optimization of these parameters will be described in detail later.

2.1 *Calculating the total coupling efficiency*

The goal of this paper is to analyze the conditions required to maximize the on-axis power coupled from the source fiber to the OF through the MMF segment. We need first to calculate the power coupled to each mode inside the OF. The total power coupled to the OF is the summation of the power in each mode. Generally, the light out of the MMF is coupled to the guided and radiating modes of the OF. Unlike the SMF–MMF case, a 100% coupling efficiency to the guided modes inside the OF is not a valid assumption. If not optimized, large portion of the light is coupled to the radiating modes.

$$1 = \sum_{v=0}^{N} \eta_{v,\mathrm{OF}} + \int_{h=0}^{\infty} \eta_{r,\mathrm{OF}}(h)\,\mathrm{d}h \tag{7}$$

and

$$\sum_{v=0}^{N} \eta_{v,\mathrm{OF}} = \sum_{v=0}^{N} \frac{\left|\int_{r=0}^{\infty}\int_{\theta=0}^{2\pi} \boldsymbol{E}_{\mathrm{MMF}}(r,\theta,z) \times H_{v,\mathrm{OF}}^{\mathrm{t}*}(r,\theta) r\,\mathrm{d}r\,\mathrm{d}\theta\right|^2}{P_{v,\mathrm{OF}} P_{\mathrm{MMF}}} \leq 1, \tag{8}$$

where h is the radiating modes index. $\eta_{v,\mathrm{OF}}$ and $\eta_{r,\mathrm{OF}}$ are the power coupling coefficients between the field at the end of the MMF and the vth guided mode and radiating mode inside the OF, respectively. $H_{v,\mathrm{OF}}^{\mathrm{t}}$ and $P_{v,\mathrm{OF}}$ are the OF vth guided mode's tangential field distribution and power, respectively. The constant N is the number of guided modes inside the OF. Notice that we used index v to indicate the guided modes inside the OF in order to differentiate from that of the guided modes inside the MMF (index j). The power at distance z, P_{MMF}, can be assumed equal to the source power, neglecting the propagation, absorption and scattering losses. Hence, the guided mode coupling efficiency is written as

$$\eta_{v,\mathrm{OF}} = \frac{\left|\int_{r=0}^{\infty}\int_{\theta=0}^{2\pi} \boldsymbol{E}_{\mathrm{MMF}}(r,\theta) \times H_{v,\mathrm{OF}}^{\mathrm{t}*}(r,\theta) r\,\mathrm{d}r\,\mathrm{d}\theta\right|^2}{P_{v,\mathrm{OF}} P_s}. \tag{9}$$

Substituting Equation (5) in Equation (9) we obtain

$$\eta_{v,\mathrm{OF}} = \frac{\left|\sum_{j=0}^{M-1} \tilde{a}_j \left(P_s/P_j\right)^{1/2} \exp\left(\mathrm{i}\beta_j z\right) \int_{r=0}^{\infty}\int_{\theta=0}^{2\pi} E_j^{\mathrm{t}}(r,\theta) \times H_{v,\mathrm{OF}}^{\mathrm{t}*}(r,\theta) r\,\mathrm{d}r\,\mathrm{d}\theta\right|^2}{P_s\, P_{v,\mathrm{OF}}}. \tag{10}$$

Equation (10) can be further simplified to

$$\eta_v = \left|\sum_{j=0}^{M-1} \tilde{a}_j \exp\left(\mathrm{i}\beta_j z\right) \left\{\frac{\int_{r=0}^{\infty}\int_{\theta=0}^{2\pi} E_j^{\mathrm{t}}(r,\theta) \times H_{v,\mathrm{OF}}^{\mathrm{t}*}(r,\theta) r\,\mathrm{d}r\,\mathrm{d}\theta}{\left(P_j\, P_{v,\mathrm{OF}}\right)^{1/2}}\right\}\right|^2. \tag{11}$$

The term in group brackets in Equation (11) is simply the modified field expansion coefficient when mapping the jth guided mode in the MMF to the vth guided mode of the OF. This coefficient is defined as $\tilde{b}_{j,v}$,

$$\tilde{b}_{j,v} = \frac{\int_{r=0}^{\infty}\int_{\theta=0}^{2\pi} E_j^{t}(r,\theta) \times H_{v,\mathrm{OF}}^{t^*}(r,\theta) r \,\mathrm{d}r \,\mathrm{d}\theta}{(P_j P_v)^{1/2}}. \tag{12}$$

Equation (11) is now simplified to

$$\eta_{v,\mathrm{OF}} = \left| \sum_{j=0}^{M-1} \tilde{a}_j \tilde{b}_{j,v} \exp(\mathrm{i}\beta_j z) \right|^2. \tag{13}$$

The total power coupled from the source to the OF through the MMF segment is then the summation of the power coupled to each mode individually.

$$\eta = \sum_{v=0}^{N-1} \left| \sum_{j=0}^{M-1} \tilde{a}_j \tilde{b}_{j,v} \exp(\mathrm{i}\beta_j z) \right|^2. \tag{14}$$

Equation (14) shows explicitly that the total coupling efficiency depends on the source excitation coefficient represented by the $\tilde{a}_j$ coefficient, the MMF length z, the modal properties of the MMF explicitly represented by the propagation constants β_j and implicitly inside the $\tilde{b}_j$ coefficient. The OF is solely represented by the $\tilde{b}_j$ coefficient. One key point to stress here is that the coupling efficiency representation in Equation (14) deals with different fibers as a collection of guided modes. The fiber geometries and material parameters are hidden in these modes' representations. The main apparent overhead in this scheme then is the generation of the modal library for the different fibers in the system. Full vectorial calculation is rigorous however, our calculations showed that the linear polarization (LP) approximation gives very close results. Under the LP approximation, the modal distributions inside the MMF have closed form formulas [12,13]. This extensively reduces the calculation time as optimizing the MMF parameters requires recalculating the modal properties of the MMF segment for each parameter change. In addition, on-axis excitation restricts a certain set of modes inside both the MMF and the OF to be excited as will be explained in the next section. This farther reduces the computation time.

2.2 *Source excitation condition: source to MMF coupling*

In our on-axis coupling scheme the input field is radially symmetric around the MMF axis. This geometry will enforce only modes with radial symmetry to be excited inside the MMF segment [8]. In other words, only first-order azimuthal modes (azimuthal index, $m = 1$) will be excited as the transverse field distributions of the zero-order and higher-order azimuthal modes have one or more sign changes along the θ direction [14]. In addition, as the phase distribution of the input beam is uniform, $\tilde{a}_j$ will have a finite value only for those first-order azimuthal modes with non-vortex phase. This constraint reduces the inner summation limit, M, in Equation (14) to half the number of the first-order guided

azimuthal modes inside the MMF. This phase constraint applies equally for the OF due to the phase matching conditions. Only first-order azimuthal modes with non-vortex phase will be excited inside the OF. This reduces the outer summation limit in Equation (14) to half the number of the first-order guided azimuthal modes in the OF, N, as well. Thus, Equation (14) can be re-written as

$$\eta = \sum_{v=0}^{N_1-1} \left| \sum_{j=0}^{M_1-1} \tilde{a}_j \tilde{b}_{j,v} \exp(\mathrm{i}\beta_j z) \right|^2, \tag{15}$$

where M_1 and N_1 are the number of the first-order guided azimuthal modes with non-vortex phase inside the MMF and the OF, respectively.

2.3 *The effect of the source size and MMF core radius*

The coupling scheme presented in this paper depends on the modulation of the complex transverse field distribution due to the interference between the guided modes (by default we mean guided first-order azimuthal modes with no vortex phase) while propagating inside the MMF segment. To guarantee a high coupling efficiency, it is required that the MMF supports a large number of modes and that most of these modes are excited in order to accurately resemble the input field distribution as shown by Equation (7) and to guarantee a high coupling (near 100%) from the SMF to the MMF (i.e. covers the N.A. of the source). The power distribution in these modes however, affects the field modulation due to the MMI.

The number of modes supported by the MMF depends on the excitation wavelength, fiber core radius and the material properties. It is always much easier to change the MMF geometry than the material properties from the fabrication perspective. For practicality reasons, we select for analysis two standard MMFs with the same material construction (fused silica cladding and Ge-doped fused silica core) and different core diameters: 62.5 and 105 μm. For these fibers the total number of guided modes is 10 and 34, respectively, as shown in Figure 2(*a*) and (*b*). As can be seen in these figures, the power coupling coefficient vanishes for each second mode. These modes are the ones with vortex phases. This agrees with the phase constraint discussed earlier. The actual numbers of excited modes, M_1, inside these two fibers are then 5 and 17, respectively. It is more practical to use the 105 μm MMF to couple the light to the OF as it supports a larger number of modes.

For fixed MMF properties the power distribution of the excited modes depends only on the shape of the input field. The input source is expected to be launched through a SMF. Changing the fiber diameter changes the effective input beam width. Figure 2(*a*) and (*b*) show the calculated power coupling efficiency for the guided modes inside the two fibers for different beam widths; 2.73, 5.4, 13 and 27.3 μm. (The last two values are hypothetical as the fibers will be multimode for these core diameter values. However, we present these values for the illustration purposes only.) For the larger beam widths (i.e. 13 and 27.3 μm), the input power is coupled mainly to very few lower order modes. This will not guarantee enough field modulation along the MMF segment and hence degrade the performance of the coupling device. The power is distributed among more

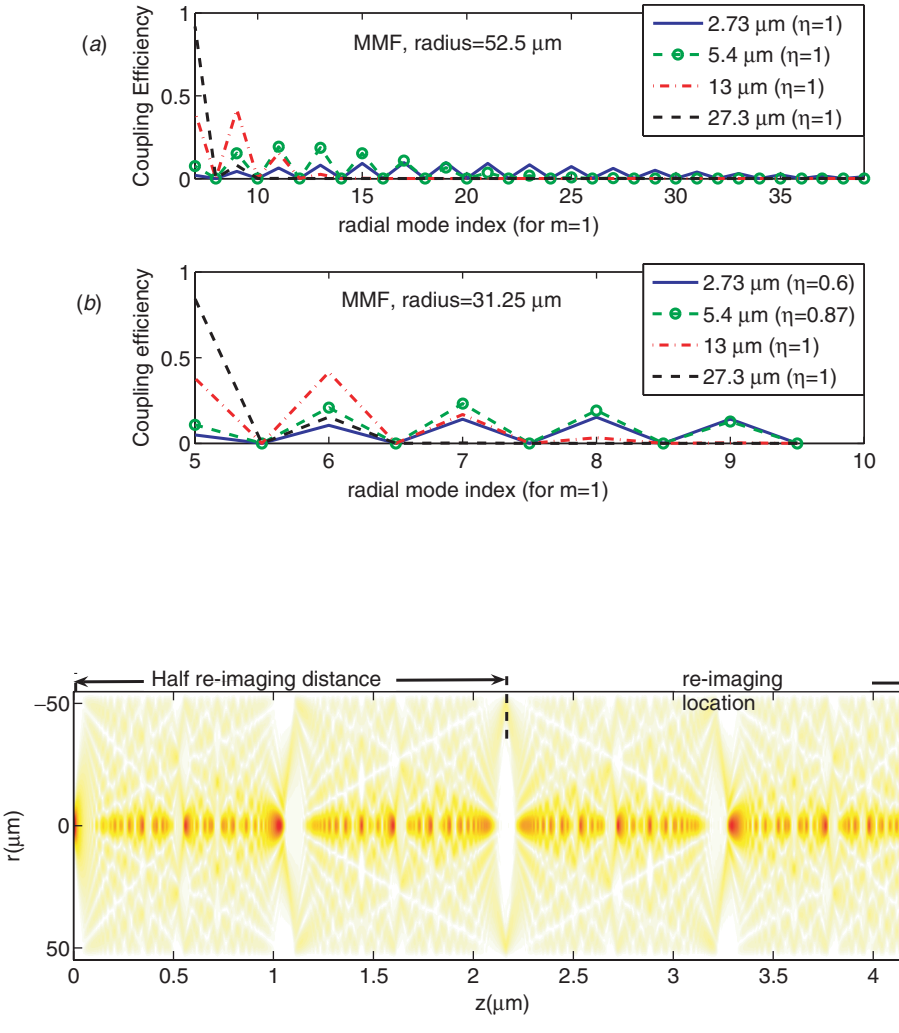

Figure 3. Calculated MMI intensity pattern inside a 105 μm MMF at a working wavelength of 1550 nm using a SMF of 9 μm diameter. (The colour version of this figure is included in the online version of the journal.)

modes for the case of the small beam widths. Hence, it is a very reasonable choice to use a standard SMF fiber with a core diameter of 8.2 μm (for which the guided mode has an effective field diameter of 10.2 μm at 1.55 μm wavelength) to couple the light to the MMF segment.

Figure 3 depicts the calculated intensity distribution inside a MMF segment when using a Corning SMF-28 as an input fiber. The length of the MMF is slightly longer than the re-imaging distance at 1550 nm excitation wavelength [5]. The intensity distribution between the half re-imaging distance and the re-imaging location is a mirror image of the first half. Thus, the MMF segment does not need to be longer than half of the re-imaging distance for the proposed scheme.

As a conclusion of this section, we have simplified the total coupling efficiency from the source to the OF using the MMF segment to the form in Equation (14). This representation requires the modal calculations of all the fibers used in the system; which can be efficiently carried out using the LP approximation. Using this representation, the calculations showed some constraints over the source excitation and the MMF geometry. Applying these constraints, the MMF parameters (core diameter and segment length) need to be further optimized in order to maximize the coupling to the OF used in the system. The next section illustrates the use of this scheme to maximize coupling to two different OF systems.

3. Coupling to cylindrically symmetric fibers

3.1 *Multimode graded index ring-shape fiber*

We now demonstrate the use of a MMF segment to maximize the total power coupling to a multimode graded index ring-shaped fiber (GRIN-RSF). The refractive index profile of this fiber is presented in Figure 4. The constants n_1, n_2, r_1 and r_2 are the maximum refractive index, cladding index, ring inner radius and ring outer radius, respectively. The values of these parameters are presented in Table 1. For this fiber, the first-order guided azimuthal mode intensity and phase distributions at a working wavelength of 1550 nm are shown in Figure 5. These fields are computed using the method presented in [8]. As seen in Figure 5, there are only four guided modes. However, two of these modes have vortex phase distributions. According to the phase constraint mentioned earlier, only modes with azimuthal index 1 and radial indices 1 and 3 will be excited.

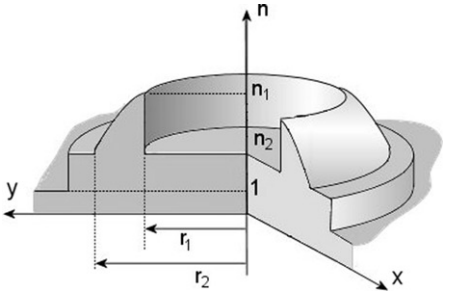

Figure 4. The GRIN-RSF refractive index profile.

Table 1. Ring-shaped graded index fiber parameters.

Parameter	Value
Graded index constant (α)	2.5
n_1 (at 1.55 μm)	1.4505
n_2 (at 1.55 μm)	1.4443
r_1	13.35 μm
r_2	25.3 μm

Using the calculated field distributions of the GRIN-RSF and MMF guided modes, Equation (15) is evaluated for values of the MMF segment length, z, between 0 and half the re-imaging distance as depicted in Figure 6. The figure shows the total power coupling efficiency to the GRIN-RSF as well as the power coupling efficiency to each of the four modes in this GRIN-RSF. The number of MMF modes in these calculations was 15 modes. It is clear from the graphs that there is no power coupled to the $(1, 0)$ and $(1, 2)$ modes inside the GRIN-RSF. These are the two modes with vortex phases and this agrees with the phase constraint mentioned above. In addition, there are three important locations marked by 1, 2 and 3. At the first location (MMF segment length $z = 3.8$ mm), the power is mainly coupled to the $(1, 1)$ mode. The calculated coupling efficiency is 0.5 (loss of 3 dB). The amount of power coupled to the $(1, 3)$ mode is minimized. At the second location ($z = 7.1$ mm), the power coupling reaches 0.5 for the $(1, 3)$ while it is minimized for the $(1, 1)$ mode. Finally, at the third location ($z = 10.65$ mm), the power coupling efficiency for the two mode peaks is 0.83 (loss of 0.8 dB). Thus, using a segment of MMF with a particular length, one can either selectively excite certain modes or maximize the total power coupled to the fiber. Although the selective coupling efficiency is low (3 dB loss) this loss can be acceptable for certain applications where the power contrast is important, such as improving the spectral response for a grating written in the GRIN-RSF.

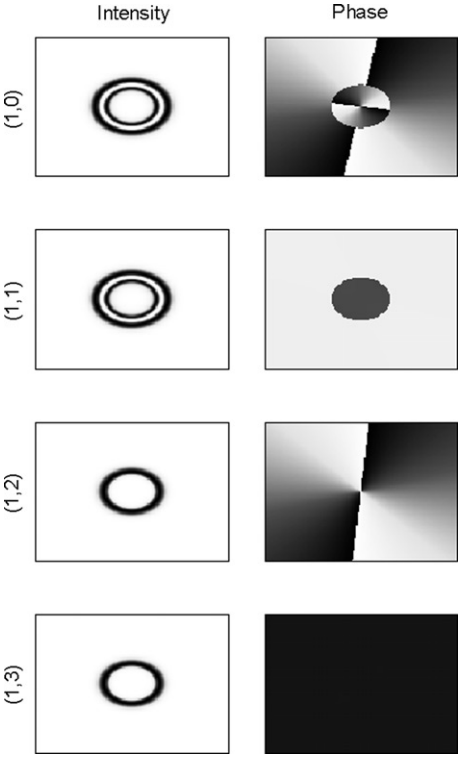

Figure 5. Intensity and phase profiles of the four guided first-order azimuthal modes inside the GRIN-RSF.

However, this paper focuses mainly on maximizing the total power coupled to the OF. The optimum MMF length for this application is then 10.65 mm (the location of the third peak in Figure 6). The fabrication error in the MMF length will cause a shift in the peak wavelength by $-149.5\,\mathrm{nm\,mm^{-1}}$ length error as shown by the linear fit of the calculated peak wavelength shift with the MMF segment length depicted in Figure 7. As shown in Equation (16) in [5], the re-imaging position is inversely proportional to the wavelength.

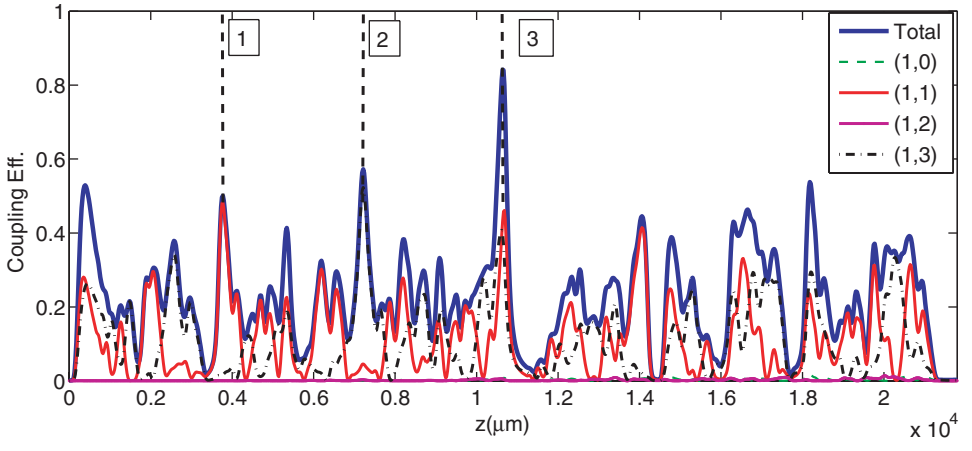

Figure 6. Calculated individual modes and total power coupling efficiencies from SMF-28 to GRIN-RSF as a function of the MMF segment length, z. (The colour version of this figure is included in the online version of the journal.)

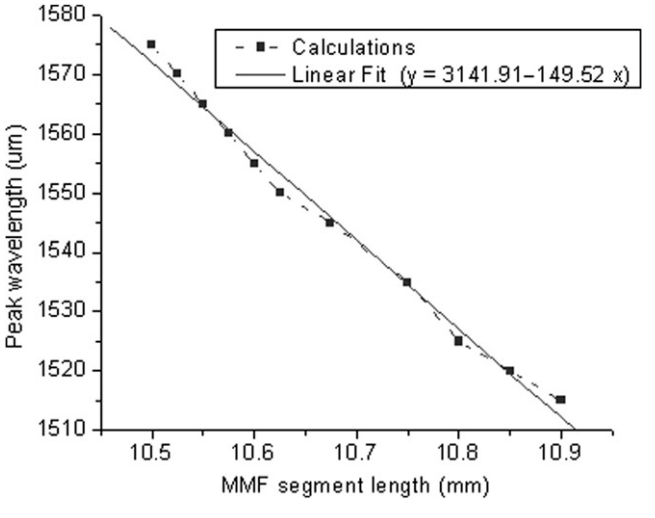

Figure 7. Calculated peak wavelength as a function of the length of the MMF segment (dashed) and the linear fit of the calculations (solid).

Accordingly, the position for peak coupling power will change in an inversely proportional manner. In order to measure the performance of the coupling device, one needs to measure the coupling efficiency versus the wavelength to locate the peak shift resulting from the fabrication error. However, this device does not require nanometre precision. According to the slope of the linear fit in Figure 7, a 1 μm error causes a shift of 0.15 nm. The graph in Figure 8 shows that the change of the coupling efficiency is slow and a 10 nm peak shift, which corresponds to 67 μm, reducing the coupling efficiency by −0.3 dB only. The required precision is then in the order of tens of microns. For this resolution, two steps of rough cleaving and fine polishing should produce sufficiently accurate devices.

In the following section, we will demonstrate experimentally on-axis coupling to a GRIN-RSF fiber when using a 10.65 mm MMF segment and show the effect of the MMF segment length on the peak wavelength.

3.2 *Experimental results*

In the experimental evaluation (as depicted in Figure 8), the source consists of a JDS tunable laser SWS15101 coupled to a standard Corning SMF-28 single mode fiber. The SMF is spliced to a 105 μm core diameter Thorlabs AFS 105/125 Y MMF, which is aimed to be cleaved to a length of 10.65 mm using a standard fiber cleaver. The error of this technique is estimated to be ±0.25 mm. The power at the output of the MMF segment is measured over the wavelength range between 1510 and 1600 nm. We used the automated moving stages in an Ericsson FSU 995 FA splicing machine to align the MMF to the GRIN-RSF for on-axis coupling measurements. The total power coupling efficiency measured at the output of the GRIN-RSF is depicted in Figure 9 (in dB) together with the theoretical results. The fabrication error results in shifting the peak towards a shorter wavelength of 1540 nm instead of the intended 1550 nm. This shows an error of 10 nm, which is a result of the MMF cleaving process. Using the linear fit in Figure 7, the estimated fiber error is 0.07 mm. Hence, the calculations were performed for a MMF segment length of 10.72 mm in order to match the measured peak wavelength. The graphs show good agreement between the measurements and the calculations. The measured peak is −1.8 dB, 1 dB less than predicted. This loss could be due to many effects. One factor is the excitation of unwanted radial modes inside the MMF due to imperfect on-axis coupling between the SMF and the MMF, and scattering losses and mode mixing inside the MMF segment. This will deform the field distribution at the end facet of the MMF and hence, reduce the total coupling efficiency. We examined the quality of the field by imaging the intensity distribution at the end facet of the MMF using a 10× objective lens and a Hamamatsu C2741 Vidicon camera. The recorded intensity distribution for a wavelength of 1540 nm is depicted in Figure 10(*b*). Figure 10(*a*) shows the calculated intensity

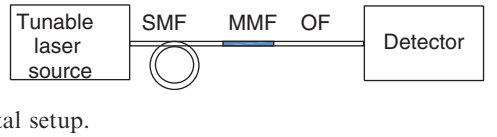

Figure 8. The experimental setup.

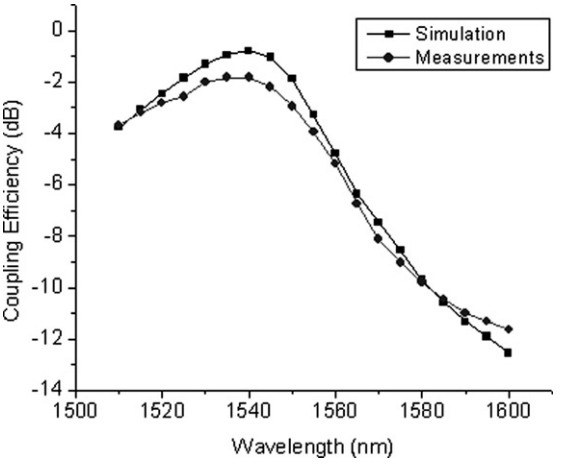

Figure 9. Measured and calculated total power coupling efficiencies from SMF-28 to GRIN-RSF through a 10.72 mm segment of 105 μm MMF as a function of the source wavelength.

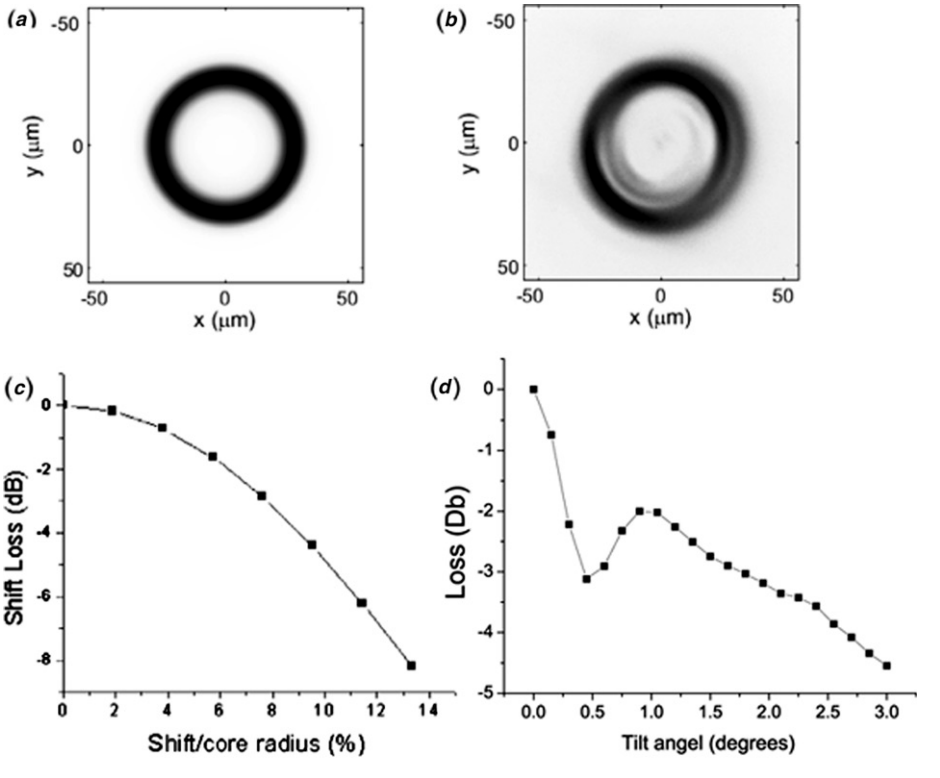

Figure 10. (*a*) Calculated intensity profile at the end facet of the MMF; (*b*) measured intensity profile at the end of the MMF; (*c*) calculated loss due to the possible shift of the SMF while splicing. (*d*) Calculated loss due to the possible tilt of the SMF while splicing.

distribution for comparison. The figures show clearly the deformation of the measured profile compared to simulations. These imperfections not only reduce the peak coupled power but also the power contrast as shown in the graphs. The degradation of the coupling efficiency due to the imperfect on-axis coupling, or shift, is depicted in Figure 10(*c*). The graph explicitly shows the automated splicing shift error is of the order of 2 μm. This shift causes a 1 dB drop as shown in the figure. This problem can be easily avoided using a better splicing tool. Another factor that might play a rule in degrading the performance of this device is the possible tilt between the two fibers when splicing. Figure 10(*d*) shows the loss as a function of tilt angle. The graph shows that the tilt in the fabricated device should be less than 0.15° for the loss to be less than or equal to 1 dB.

3.3 *Concentric-shells multimode fiber*

As a demonstration of the generality of this method, we present here theoretical calculations of the proposed coupling scheme when using a different OF system. The fiber consists of four concentric shells of refractive indices higher than the cladding and the regions in between as depicted in Figure 11(*a*). Each shell has a specific width, $t = 2.5\,\mu m$, and separation, $D = 6.3\,\mu m$ and an inner radius of 15.8 μm. This fiber serves as a multimode fiber but at the same time the modal propagation characteristics are tailored to facilitate the creation of a narrow band fiber Bragg grating. Figure 11(*b*) depicts the intensity profiles of the first-order azimuthal modes with non-vortex phase for this fiber calculated using the approach in [8]. The calculations in Figure 12 show that maximum achievable coupling efficiency between SMF and SF changes with the MMF core radius. The maximum coupling efficiency for each core radius is achieved at a different MMF length. A MMF with 50 μm radius seems to have the highest maximum achievable coupling efficiency. Figure 13 shows the calculated total coupling efficiency between the SMF and the OF when using a 50 μm radius MMF over a half re-imaging distance. The graph shows a maximum coupling efficiency of 93% (−0.32 dB loss) at location 1. The calculated coupling efficiencies for the other two locations are 82% and 84%.

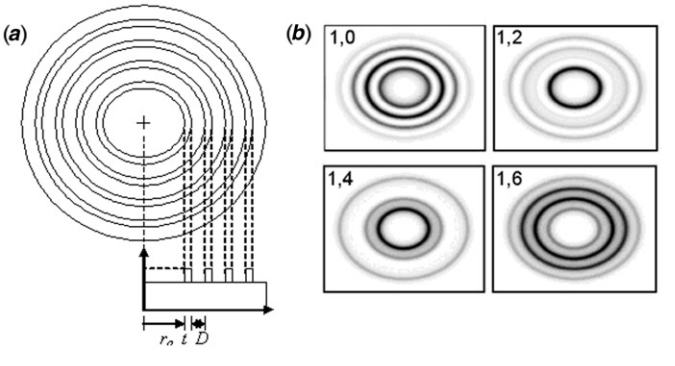

Figure 11. (*a*) Concentric multi-shell fiber structure; (*b*) intensity distributions of the guided first-order azimuthal modes with non-vortex inside this structure.

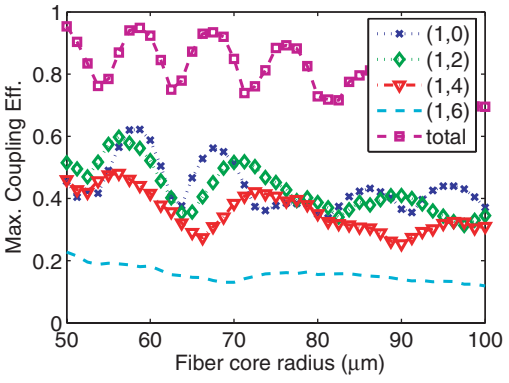

Figure 12. The maximum achievable coupling efficiency from SMF to the multi-shell fiber as a function of the MMF core radius. (The colour version of this figure is included in the online version of the journal.)

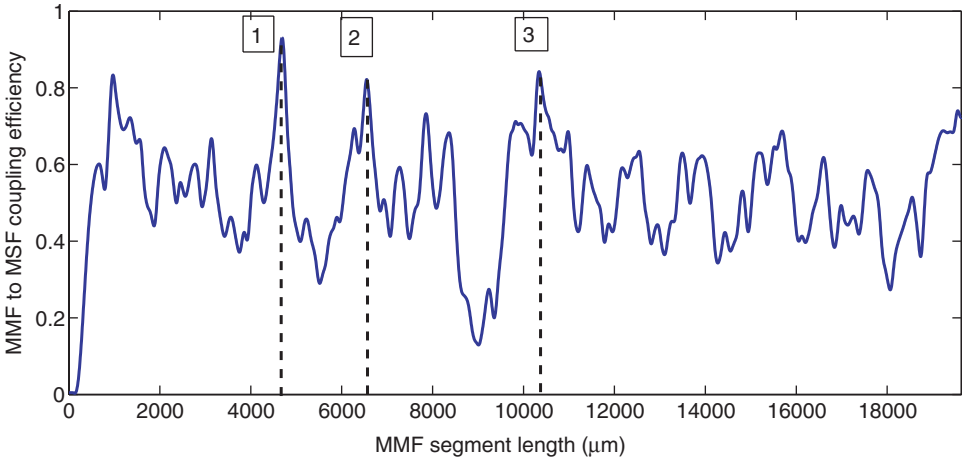

Figure 13. Calculated total coupling efficiency to the multi-shell fiber as a function of a 50 μm MMF segment length. (The colour version of this figure is included in the online version of the journal.)

4. Conclusions

We demonstrated a simple, novel method to maximize power coupling to a SF. The method is based on the MMI effect in a MMF segment inserted between the source fiber and the SF. In order to design an optimized MMF segment we have derived a simplified representation for the total power coupling efficiency. The formula links the coupling efficiency to the source excitation condition, MMF parameters and the coupling between the different MMF and SF modes. The total power coupling efficiency to a GRIN-RSF is calculated as a function of the MMF length. The calculations showed a peak coupling efficiency of 83% (loss of −0.8 dB) for a 10.72 mm MMF segment at an operation wavelength of 1540 nm. We attribute the difference between the measured and intended

peak wavelength to fabrication errors of the MMF length. We found a good agreement between experimental results and theoretical predictions over a wide wavelength range. The measured peak coupling efficiency is lower, due to an imperfect field distribution at the end of the MMF segment caused by excitation of higher order modes. As a demonstration of the generality of this scheme to maximize coupling to radially symmetric optical fiber, we applied this scheme to a four concentric-shell fiber. The predicted coupling efficiency for different MMF parameters is 93%.

References

[1] Yamauchi, R. Specialty Fibers. *Lasers and Electro-Optics Society Annual Meeting IEEE;* IEEE: Piscataway, NJ, 1994; pp. 228–229.
[2] Nubling, R.K.; Harrington, J.A. *Appl. Opt*. **1996,** *35,* 372–380.
[3] Nguyen, M.; Irwin, B.S.; Higbee, R.G.; Mohammed, W.S.; Johnson, E.G.; Bartels, K.E.; Warren, W.L.; Church, K.H. *Proc. SPIE* **2004,** *5317,* 22–28.
[4] Mehta, A.; Mohammed, W.; Johnson, E.G. *Photon. Technol. Lett*. **2004,** *15,* 1129–1131.
[5] Johnson, E.G.; Stack, J.; Koehler, C. *J. Lightwave Technol*. **2001,** *19,* 753–758.
[6] Mohammed, W.S.; Mehta, A.; Pitchumani, M.; Johnson, E.G. *Photon. Technol. Lett*. **2005,** *17,* 1441–1443.
[7] Soldano, L.B.; Pennings, E.C.M. *J. Lightwave Technol*. **1995,** *13,* 615–627.
[8] Mohammed, W.S.; Mehta, A.; Johnson, E.G. *J. Lightwave Technol*. **2004,** *22,* 469–477.
[9] Selvas, R.; Torres-Gomez, I.; Martinez-Rios, A.; Alvarez-Chavez, J.A.; May-Arrioja, D.A.; LiKamWa, P.; Mehta, A.; Johnson, E.G. *Opt. Express* **2005,** *13,* 9439–9445.
[10] Sanchez, G.; Martinez-Rios, A.; May-Arrioja, D.; Torres-Gomez, I.; Alvarez-Chavez, J. *Electron. Lett*. **2006,** *42,* 1337–1338.
[11] Li, E.B.; Wang, X.L.; Zhang, C. *Appl. Phys. Lett*. **2006,** *89,* 091119.
[12] Kawano, K.; Kitoh, T. Analytical Methods: Method for an Optical Fiber. In *Introduction to Optical Waveguide Analysis;* Wiley: New York, 2001; pp. 36–54.
[13] Okamoto, K. *Fundamentals of Optical Waveguides;* Academic Press: New York, 2000.
[14] Mohammed, W.; Gu, X.; Smith, P.W.E. *Appl. Opt*. **2006,** *45,* 3307–3316.
[15] Yariv, A.; Yeh, P. *Optical Waves in Crystals: Propagation and Control of Laser Radiation;* Wiley Interscience: New York, 1984.

Appendix A: multimode interference in MMF

Modes supported by any lossless waveguide with arbitrary structure has the following orthogonality property [15], pp. 408–410:

$$\iint \left(E_1 \times H_2^*\right) \circ a_z \, \mathrm{d}a = 0. \tag{A1}$$

In Equation (A1), $E_{1,2}$, and $H_{1,2}$ are the electric field and magnetic field for two different modes (subscripts 1 and 2), respectively. da is the unit area and $\circ$ is the dot product. The dot product is finite only for the z components of the cross-product in Equation (A1). Hence, Equation (A1) can be re-written in terms of the tangential components of the fields only.

$$\iint \left(E_1^{\mathrm{t}} \times H_2^{\mathrm{t}^*}\right) \mathrm{d}a = 0. \tag{A2}$$

The superscript 't' indicates the transverse field components and the asterisk represents the complex conjugate. As mentioned earlier, the transverse electric field components of the source field can be expanded in terms of the guided modes' transverse field components, E_j^{t}, as follows

$$\boldsymbol{E}_{\mathrm{s}}(r,\theta) = \sum_{j=0}^{M} a_j \, E_j^{\mathrm{t}}(r,\theta). \tag{A3}$$

M is the total number of guided modes and a_j is the MMF jth mode excitation coefficient. Multiplying (cross-product) both sides of Equation (A3) by the conjugate of the MMF hth mode transverse magnetic field, $H_h^{\mathrm{t}^*}$, and carrying a two-dimensional integration over the area, Equation (A3) is written as

$$\int_{r=0}^{\infty}\int_{\theta=0}^{2\pi} \left(\boldsymbol{E}_{\mathrm{s}}(r,\theta) \times H_h^{\mathrm{t}^*}(r,\theta)\right) r \, \mathrm{d}r \, \mathrm{d}\theta = \sum_{j=0}^{M} a_j \int_{r=0}^{\infty}\int_{\theta=0}^{2\pi} \left(E_j^{\mathrm{t}}(r,\theta) \times H_h^{\mathrm{t}^*}(r,\theta)\right) r \, \mathrm{d}r \, \mathrm{d}\theta. \tag{A4}$$

Using the orthogonality relation in (A2), the right-hand side of Equation (A4) is finite only when $j = h$. This results in the following relation for the excitation coefficient:

$$a_h = \frac{\int_{r=0}^{\infty}\int_{\theta=0}^{2\pi} \boldsymbol{E}_{\mathrm{s}}(r,\theta) \times H_h^{\mathrm{t}^*}(r,\theta) r \, \mathrm{d}r \, \mathrm{d}\theta}{P_h}. \tag{A5}$$

The mode power, P_h, is defined as

$$P_h = \int_{r=0}^{\infty}\int_{\theta=0}^{2\pi} \left(E_h^{\mathrm{t}}(r,\theta) \times H_h^{\mathrm{t}^*}(r,\theta)\right) r \, \mathrm{d}r \, \mathrm{d}\theta. \tag{A6}$$

Similarly, using the magnetic field expansion of the source, we obtain an equivalent relation for the excitation coefficient

$$a_h = \frac{\int_{r=0}^{\infty}\int_{\theta=0}^{2\pi} \boldsymbol{H}_{\mathrm{s}}(r,\theta) \times E_h^{\mathrm{t}^*}(r,\theta) r \, \mathrm{d}r \, \mathrm{d}\theta}{P_h}. \tag{A7}$$

Hence,

$$\int_{r=0}^{\infty}\int_{\theta=0}^{2\pi} \boldsymbol{H}_{\mathrm{s}}(r,\theta) \times E_h^{\mathrm{t}^*}(r,\theta) r \, \mathrm{d}r \, \mathrm{d}\theta = \int_{r=0}^{\infty}\int_{\theta=0}^{2\pi} \boldsymbol{E}_{\mathrm{s}}(r,\theta) \times H_h^{\mathrm{t}^*}(r,\theta) r \, \mathrm{d}r \, \mathrm{d}\theta. \tag{A8}$$

The power coupling coefficient can be obtained by first multiplying (cross-product) both sides of Equation (A2) by the conjugate of the source transverse magnetic field, $\boldsymbol{H}_{\mathrm{s}}^*$, and carrying a double integral over the area, we get the following relation:

$$\int_{r=0}^{\infty}\int_{\theta=0}^{2\pi} \left(\boldsymbol{E}_{\mathrm{s}}(r,\theta) \times \boldsymbol{H}_{\mathrm{s}}^*(r,\theta)\right) r \, \mathrm{d}r \, \mathrm{d}\theta = \sum_{j=0}^{M} a_j \int_{r=0}^{\infty}\int_{\theta=0}^{2\pi} \left(E_j^{\mathrm{t}}(r,\theta) \times \boldsymbol{H}_{\mathrm{s}}^*(r,\theta)\right) r \, \mathrm{d}r \, \mathrm{d}\theta \tag{A9}$$

The left-hand side of Equation (A7) is the source power, P_s. Using the definition of the excitation coefficient, a_h, in (A5) and the relation in (A7), Equation (A8) can be written as

$$P_s = \sum_{j=0}^{M} \frac{\int_{r=0}^{\infty}\int_{\theta=0}^{2\pi} \boldsymbol{E}_{\mathrm{s}}(r,\theta) \times H_j^{\mathrm{t}^*}(r,\theta) r \, \mathrm{d}r \, \mathrm{d}\theta}{P_j} \int_{r=0}^{\infty}\int_{\theta=0}^{2\pi} \boldsymbol{E}_{\mathrm{s}}^*(r,\theta) \times H_h^{\mathrm{t}}(r,\theta) r \, \mathrm{d}r \, \mathrm{d}\theta. \tag{A10}$$

Dividing both sides of Equation (A9) by P_s

$$1 = \sum_{j=0}^{M} \frac{\left| \int_{r=0}^{\infty} \int_{\theta=0}^{2\pi} \boldsymbol{E}_{\mathrm{s}}(r, \theta) \times H_j^{*}(r, \theta) r \, \mathrm{d}r \, \mathrm{d}\theta \right|^2}{P_j P_s} = \sum_{j=0}^{M} \eta_j. \tag{A11}$$

The coefficient, η_j, is the amount of power coupled to each guided mode, or the power coupling coefficient.